Probing the evolution of quantum superposition states in a nuclear spin-5/2 system

Byoung Jin Suh,[1] Ferdinando Borsa,[2] and Seung-Ho Baek[3,*]

[1]*Department of Physics, The Catholic University of Korea, Bucheon 14662, Republic of Korea*

[2]*Ames Laboratory, U.S. Department of Energy and Department of Physics and Astronomy, Iowa State University, Ames, Iowa 50011, USA*

[3]*Department of Physics, Changwon National University, Changwon 51139, Republic of Korea*

(Received 7 April 2023; accepted 2 August 2023; published 15 August 2023)

We report the effects of off-diagonal coupling on eigenstates and eigenvalues of a realistic quantum Hamiltonian, a ^{121}Sb (spin $I = 5/2$) nuclear spin Hamiltonian in an antimony single crystal. In our nuclear resonance experiment, off-diagonal matrix elements are generated and controlled by the angle θ between the directions of the electric field gradient and an external magnetic field. With a very small θ, a two-state-like avoided level crossing is directly probed as a function of an external magnetic field. On the other hand, by increasing θ under a weak magnetic field, we find that the nuclear spin transitions undergo dramatic changes as θ approaches 90°. All our experimental observations are in excellent agreement with exact diagonalization calculations for the Hamiltonian, demonstrating how superposition states of a multistate quantum system evolve as a function of a well-defined control parameter.

DOI: 10.1103/PhysRevResearch.5.033105

I. INTRODUCTION

The von Neumann–Wigner theorem [1–4], often referred to as the noncrossing rule, states that any two eigenvalues for a Hamiltonian cannot be degenerate unless the two corresponding eigenstates have different symmetries. As a result, linear superpositions of degenerate eigenstates, i.e., having the same symmetry, lead to an avoided crossing of energy levels in close proximity. This theorem is indeed fundamental to numerous quantum phenomena, including quantum resonance in molecules [5], the Landau-Zener effect [6], topological band crossings in solids [7], Rabi oscillations [8,9], and macroscopic quantum tunneling of distinct states [10–14]. Despite the widespread applicability and usefulness of the von Neumann–Wigner theorem in various fields, an experimental challenge remains in investigating the evolution of unperturbed basis states towards coherent superposition states as a function of a control parameter, being essential for quantitatively understanding the effects of the theorem on an isolated quantum system. The difficulty lies in finding a real quantum system that fulfills the following prerequisites: (i) isolated multiple basis states, (ii) easily tunable off-diagonal coupling, and (iii) an energy scale accessible by an experimental setup for both diagonal and off-diagonal matrix elements.

A nuclear spin system does meet these criteria, since nuclear spins in a solid behave as an ensemble of coupled particles with well-defined energy levels [15,16]. When nuclei with spins greater than 1/2, thus possessing a quadrupole moment, are placed in an axially symmetric electric field gradient (EFG), the nuclear quadrupole interaction, in the absence of an external magnetic field **H**, has its spins quantized in the direction of the EFG. By applying **H** that are not parallel to the principal component EFG tensor, tunable off-diagonal matrix elements can be generated [17–21]. The crucial task for our experiment is then to find a suitable nuclear spin system in which the quadrupole interaction has the right energy scale relative to the Zeeman one in order to achieve superposition states with like symmetry by mixing the initial basis states. After an extensive search for a quadrupolar spin system, we have chosen antimony metal [22,23] as the best candidate material for our purpose, since the ^{121}Sb isotope in the metal has a suitable and comparable strength of both quadrupole and Zeeman interactions, enabling us to drive the nuclear spin energy levels to intersect by applying small external magnetic fields.

II. EXPERIMENTAL DETAILS

A high-quality Sb single crystal (approximately $12 \times 4 \times 2$ mm^3) acquired from MaTecK GmbH (Germany) was cooled to 4.2 K in a liquid helium bath cryostat. ^{121}Sb (nuclear spin $I = 5/2$) nuclear magnetic resonance (NMR)–nuclear quadrupole resonance (NQR) experiments were carried out using a TecMag spectrometer in a variable resistive magnet. In order to control the angle between the c axis of the crystal and an external magnetic field, the bath cryostat was manually rotated. The ^{121}Sb NMR spectra were obtained by a standard spin-echo technique with a typical $\pi/2$ pulse length of 2–3 μs.

III. RESULTS

A. Exact diagonalization calculations

Figure 1(a) shows the trigonal (space group $R\bar{3}m$) crystal structure of antimony [22]. Since the Sb atoms have an axial symmetry about the c axis, the EFG V_{zz} at the Sb nuclear

*shbaek@changwon.ac.kr

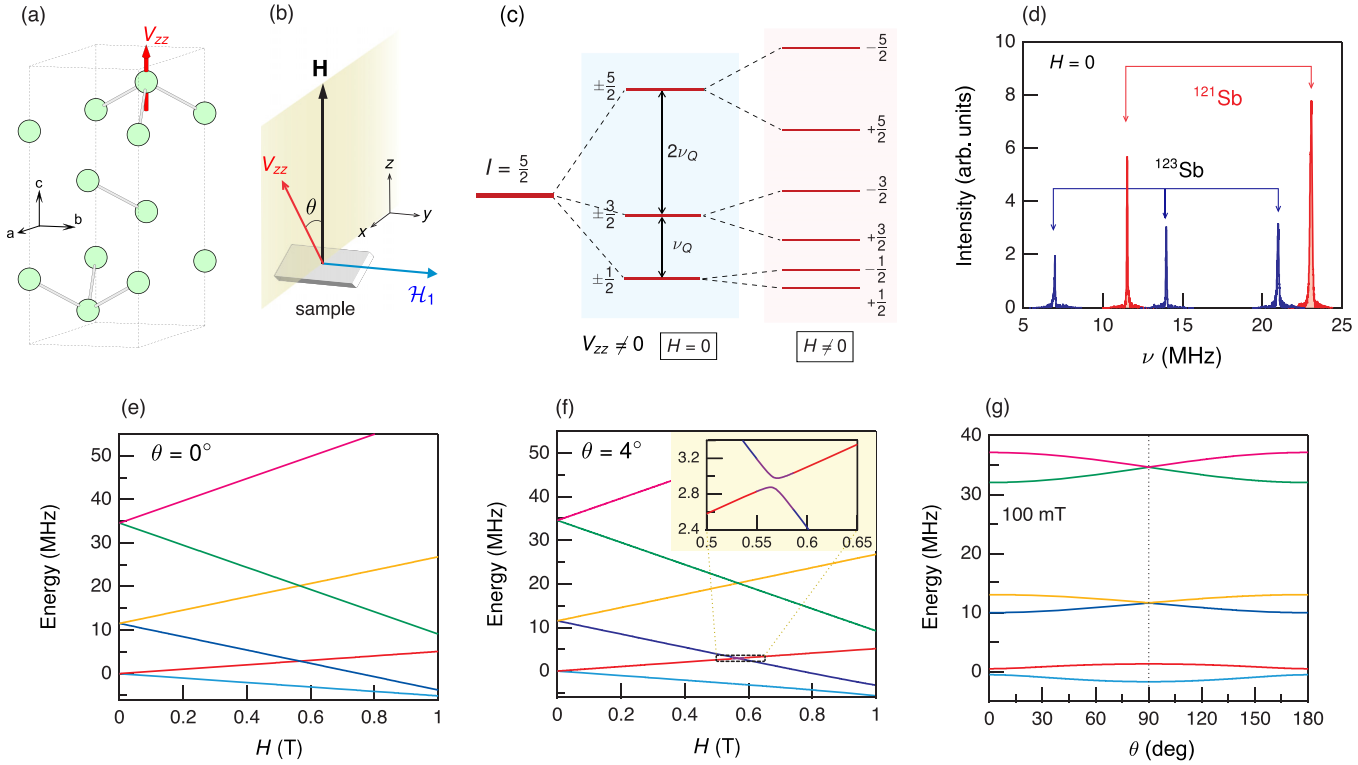

FIG. 1. (a) Crystal structure of Sb. An axially symmetric electric field gradient V_{zz} is along c at the nuclear site. (b) The angle θ between V_{zz} and an external field H in the xz plane can be controlled by rotating the crystal around the y axis. The radio-frequency field $\mathcal{H}_1$, which induces transitions between the energy levels, is applied along the y axis. (c) Schematic diagram of the quadrupole and Zeeman energy splitting for $I = 5/2$ with a finite V_{zz} in an axial symmetry and $\mathbf{H} = H\hat{z}$. (d) The NQR spectrum for ^{121}Sb ($I = 5/2$) measured at 4.2 K, which yields $\nu_Q = 11.527$ MHz. The spectrum for the isotope ^{123}Sb ($I = 7/2$) is also shown. [(e)–(g)] Energy level diagrams obtained by exact diagonalization calculations. The spin states (either $|m\rangle$ or $|m'\rangle$) of the levels just after the Zeeman splitting are in the same order as those in the diagram on the right-hand side of (c). (e) For $\theta = 0^\circ$ ($V_{zz} \parallel H$), a pure level crossing takes place. (f) For $\theta = 4^\circ$, the level repulsion between the $|-\frac{1}{2}\rangle$ and $|+\frac{3}{2}\rangle$ states is observed, as emphasized in the inset. (g) Angular dependence of the energy levels at $H = 100$ mT.

site is parallel to the c direction [23]. When $\mathbf{H} = 0$, the EFG partially lifts the sixfold degenerate nuclear spin levels of ^{121}Sb to three doublets separated by integer multiples of the quadrupole frequency $\nu_Q \equiv 3eQV_{zz}/2I(2I-1)h$, where e is the electron charge, Q is the nuclear quadrupole moment, and h is the Planck constant, as shown in Fig. 1(c). The application of $\mathbf{H}$ lifts the remaining degeneracy by producing a Zeeman splitting of the quadrupole doublets as shown in Fig. 1(c). The total nuclear Hamiltonian is given by [24]

$$\mathcal{H} = -\gamma\hbar\hat{\mathbf{I}}\cdot\mathbf{H} + \frac{h\nu_Q}{6}\left(3\hat{I}_z^2 - \hat{I}^2\right), \tag{1}$$

where γ is the nuclear gyromagnetic ratio and $\hat{I}$ is the nuclear spin operator. In our experimental setup, $\mathbf{H} = H\hat{z}$ and the crystal can be rotated in order to control the angle θ between V_{zz} and H as illustrated in Fig. 1(b).

The ^{121}Sb NQR spectrum obtained in zero field is shown in Fig. 1(d), in which the resonance frequencies correspond to ν_Q and $2\nu_Q$ [see Fig. 1(c)]. The linewidth of the spectrum is about 80 kHz, which sets the resolution limit of our experiment. The NQR spectrum of the other isotope ^{123}Sb is also shown for comparison, which is composed of three equally spaced resonance frequencies consistent with the larger nuclear spin $I = 7/2$ and a smaller ν_Q. In the present study we focus solely on ^{121}Sb.

Using the experimentally obtained $\nu_Q = 11.527$ MHz, we calculate the nuclear spin energy eigenvalues of ^{121}Sb (in frequency units) as a function of H and θ by the exact diagonalization (ED) of the Hamiltonian (1). The results are presented in Figs. 1(e) and 1(f) for $\theta = 0^\circ$ and 4°, respectively. For $\theta = 0^\circ$, the energy levels intersect without affecting one another (level crossing), in agreement with the diagonalized Hamiltonian. For $\theta = 4^\circ$, an avoided crossing is found between the energy levels associated with the $|-\frac{1}{2}\rangle$ and $|+\frac{3}{2}\rangle$ states [see the inset of Fig. 1(f)], while other energy levels show nearly pure level crossings within the resolution limit of 80 kHz. Indeed, the ED calculations show that only the two lower-energy states are significantly mixed, forming the mixed states of approximately $0.70|-\frac{1}{2}\rangle \pm 0.69|+\frac{3}{2}\rangle$ at 0.567 T where the two energy levels are closest to each other, with negligible mixing with other states. Interestingly, the mixed states are very close to symmetric and antisymmetric superpositions of $|-\frac{1}{2}\rangle$ and $|+\frac{3}{2}\rangle$, i.e., $\frac{1}{\sqrt{2}}(|-\frac{1}{2}\rangle \pm |+\frac{3}{2}\rangle)$. The two-state-like superposition states are also formed for $\theta < 4^\circ$ with a reduced level separation, whereas they are progressively contaminated by other basis states as θ is increased away from 4°. Hence, we attribute the two-state-like behavior to the weak off-diagonal coupling limit ($\theta \leqslant 4^\circ$).

In order to investigate the effect of strong off-diagonal coupling on the system, the angular dependence of energy

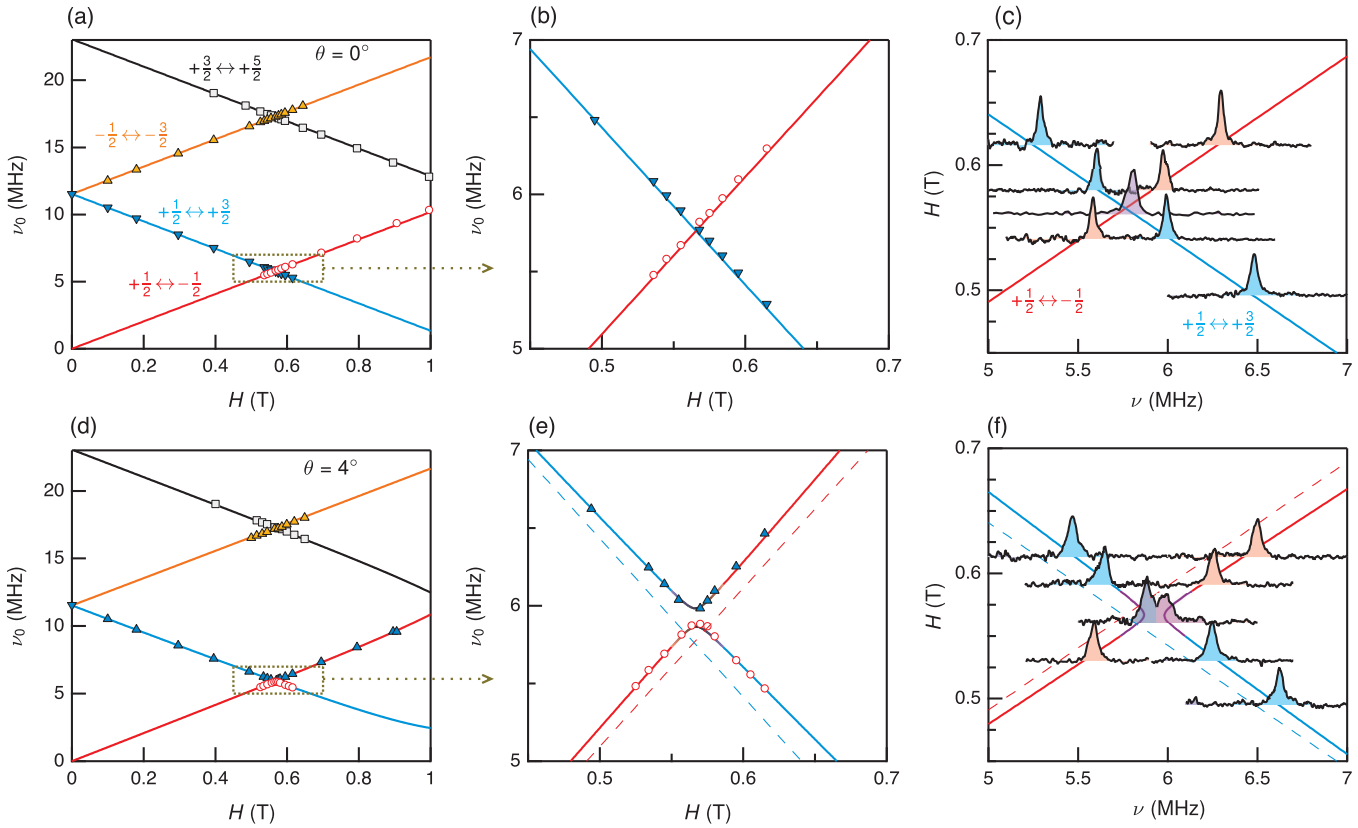

FIG. 2. The ^{121}Sb NMR frequencies ν_0 as a function of H measured at 4.2 K for [(a)–(c)] $\theta = 0^\circ$ and [(d)–(f)] $\theta = 4^\circ$. The solid lines are the nuclear transitions allowed by the selection rule, obtained from the energy eigenvalues depicted in Figs. 1(e) and 1(f). The dotted rectangle regions in (a) and (d) are enlarged in (b) and (e), in order to show clearly the pure level crossing for $\theta = 0^\circ$ compared with the avoided crossing for $\theta = 4^\circ$. Selected NMR spectra for the data in (b) and (e) are shown in (c) and (f), respectively, where the axes are interchanged. The dashed lines in (e) and (f) denote the unperturbed resonance frequencies calculated for $\theta = 0^\circ$.

eigenvalues is calculated at a fixed magnetic field of 100 mT, as shown in Fig. 1(g). Note that the basis states $|m\rangle$ chosen for $\theta = 0^\circ$ evolve into superposition states $|m'\rangle$ when $\theta > 0^\circ$. It is worth stressing that we do not add an external perturbation to the Hamiltonian but modify the internal parameter θ of the otherwise diagonalized Hamiltonian on the basis states $|m\rangle$ to generate off-diagonal matrix elements. A peculiar feature is that the energy splitting between the $|\pm\frac{1}{2}'\rangle$ states increases with increasing θ becoming maximal at 90°, while the splitting for two other doublets $|\pm\frac{3}{2}'\rangle$ and $|\pm\frac{5}{2}'\rangle$ becomes minimal at 90°.

B. Experimental results and discussion

Now we present our experimental results and compare them with the above ED calculations. The ^{121}Sb NMR frequencies ν_0, which are equivalent to the nuclear transition energies obeying the selection rule $\Delta m = \pm 1$, are depicted in Figs. 2(a) and 2(d) as a function of H for $\theta = 0^\circ$ and 4°, respectively. Figures 2(b) and 2(e) offer an enlarged view of the dotted rectangle regions in Figs. 2(a) and 2(d), respectively, and selected raw spectra are presented in Figs. 2(c) and 2(f). For $\theta = 0^\circ$, the ν_0 values change linearly with H through the level crossing field, being well described by the calculated transitions (solid lines). In contrast, for $\theta = 4^\circ$, we observe a clear repulsive behavior between the transitions $+\frac{1}{2} \leftrightarrow -\frac{1}{2}$ and $+\frac{1}{2} \leftrightarrow +\frac{3}{2}$ as shown in Figs. 2(e) and 2(f), whereas other transitions with larger resonance frequencies appear to intersect each other like for $\theta = 0^\circ$. This is precisely because an avoided level crossing occurs only between the $|-\frac{1}{2}\rangle$ and $|+\frac{3}{2}\rangle$ states as predicted in the inset of Fig. 1(f). Note that the ν_0 values for $\theta = 4^\circ$ are clearly increased in comparison with those for $\theta = 0^\circ$ [dashed lines in Figs. 2(e) and 2(f)]. These results imply that a very small off-diagonal coupling tends to generate linear superpositions of low-lying intersecting states selectively, resulting in the two-state-like avoided crossing.

Having illustrated the influence of a small off-diagonal coupling on eigenstates, we now aim to unravel the various potential results when the off-diagonal coupling becomes strong, i.e., θ is large. For simplicity, we focus on the transitions which involve the $|\pm\frac{1}{2}'\rangle$ and $|\pm\frac{3}{2}'\rangle$ states. The ^{121}Sb NMR spectra measured at $H = 100$ mT are displayed in Fig. 3(a) as a function of θ. The Zeeman-split NMR peaks at $\theta = 0^\circ$ follow the angular dependence of the resonance frequencies computed for $+\frac{1}{2}' \leftrightarrow +\frac{3}{2}'$ and $-\frac{1}{2}' \leftrightarrow -\frac{3}{2}'$. Roughly at $\theta > 20^\circ$, we detect emerging NMR peaks whose intensity grows with increasing θ at the expense of the intensity of other two peaks. Since the calculated transitions among the energy levels in Fig. 1(g) are in perfect agreement with the

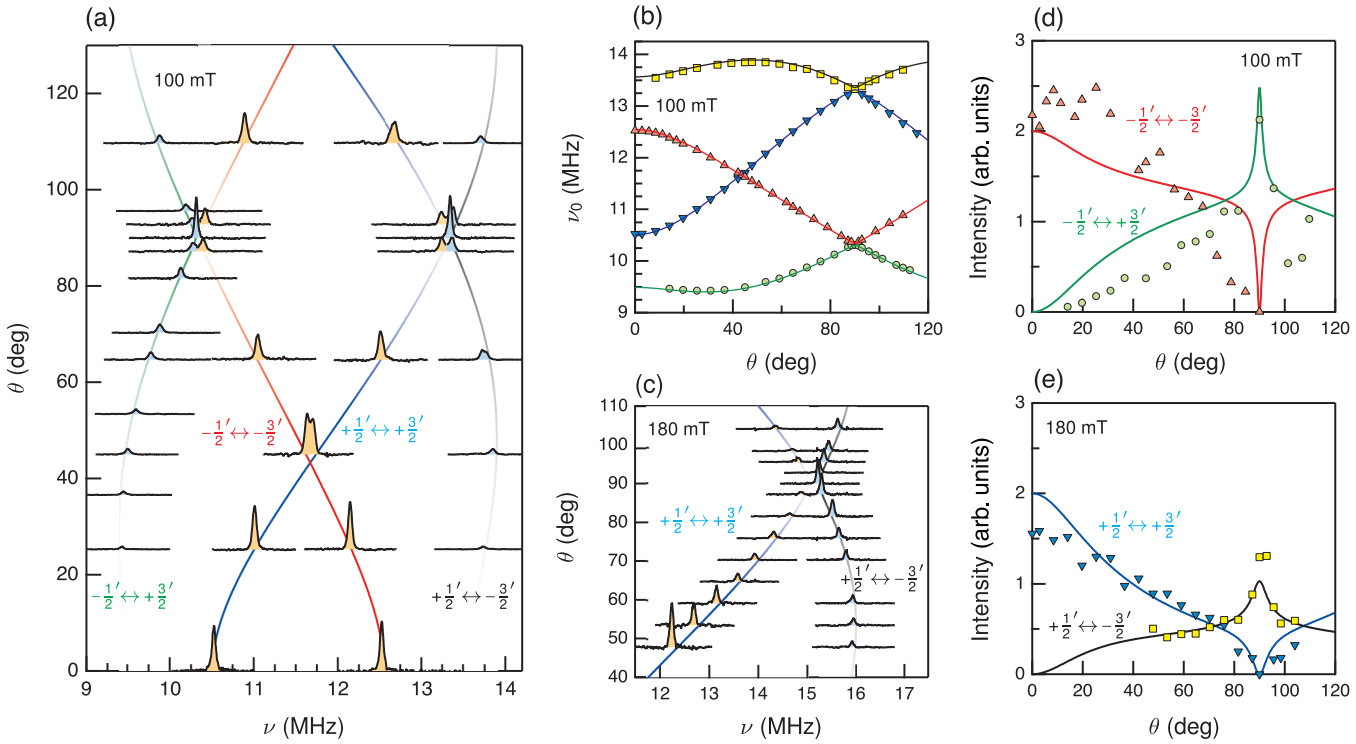

FIG. 3. (a) Selected NMR spectra associated with the transitions between the $|\pm\frac{1}{2}'\rangle$ and $|\pm\frac{3}{2}'\rangle$ states as a function of θ measured at 100 mT. Due to the mixing of basis states, the otherwise forbidden transitions (leftmost and rightmost spectra) are allowed, yielding four transitions at $0^\circ < \theta < 90^\circ$. The color density of each line indicates the transition probability $W_{ij} = |\langle m_i'|I_y|m_j'\rangle|^2$. Note that the transitions $-\frac{1}{2}' \leftrightarrow -\frac{3}{2}'$ and $+\frac{1}{2}' \leftrightarrow +\frac{3}{2}'$ vanish at 90°. (b) Angle dependence of the NMR frequencies ν_0 at 100 mT. The solid lines represent ED calculations. (c) The NMR spectra for the $+\frac{1}{2}' \leftrightarrow \pm\frac{3}{2}'$ transitions as a function of θ measured at 180 mT. The NMR signal intensity is shown as a function of θ for (d) the transition $-\frac{1}{2}' \leftrightarrow \pm\frac{3}{2}'$ at 100 mT and (e) the transition $+\frac{1}{2}' \leftrightarrow \pm\frac{3}{2}'$ at 180 mT. The solid lines denote W_{ij}.

resonance frequencies of the four NMR peaks [see Fig. 3(b)], we conclude that the new NMR peaks arise from the otherwise forbidden transitions $\pm\frac{1}{2}' \leftrightarrow \mp\frac{3}{2}'$. It is remarkable that at 90° the signal intensity for $\pm\frac{1}{2}' \leftrightarrow \pm\frac{3}{2}'$ vanishes whereas that for $\pm\frac{1}{2}' \leftrightarrow \mp\frac{3}{2}'$ reaches a maximum [see Fig. 3(a)].

The contrasting behavior of the NMR signal intensities near 90° is confirmed by measuring the transitions $+\frac{1}{2}' \leftrightarrow \pm\frac{3}{2}$ at the higher field of 180 mT, as shown in Fig. 3(c). A frequency gap is apparent at 90°, indicating that the energy splitting between $|\pm\frac{3}{2}'\rangle$, which is barely visible at 100 mT [see Fig. 1(g)], increases with increasing H. Moreover, as seen in Figs. 3(a) and 3(c), the identification of the two peaks at 90° as distinct from the two at 0°, i.e., the former not resulting from the shifting of the latter, is very revealing. Without following the complete angular dependence of the NMR spectra as shown in Fig. 3(a), it would have been challenging to discern this subtle but important difference.

Figures 3(d) and 3(e) show the integrated NMR signal intensity as a function of θ for the transitions $-\frac{1}{2}' \leftrightarrow \pm\frac{3}{2}'$ at 100 mT and $+\frac{1}{2}' \leftrightarrow \pm\frac{3}{2}'$ at 180 mT, respectively. The solid lines are the calculated transition probabilities $W_{ij} = \frac{2\pi}{\hbar}|\langle m_i'|\mathcal{H}_1|m_j'\rangle|^2 \propto |\langle m_i'|\hat{I}_y|m_j'\rangle|^2$ to which the experimental data are scaled. The W_{ij} values are also expressed as color gradation in Figs. 3(a) and 3(c). The theoretical curves are in fair agreement with the experimental data, capturing well the contrasting behavior of the NMR signal intensities near 90°, even though we do not make experimental corrections to the signal intensity such as the T_2 effect or the frequency dependence of the transmitted power. In particular, the zero transition probabilities for $\pm\frac{1}{2}' \leftrightarrow \pm\frac{3}{2}'$ at 90° account for the disappearance of the relevant NMR peaks.

Further, the ED calculations reveal that the six eigenstates become superpositions of three basis vectors at $\theta = 90^\circ$ as shown below, whereas otherwise they consist of all six basis vectors:

$$
\begin{aligned}
|+\tfrac{1}{2}'\rangle &= -0.46|+\tfrac{1}{2}\rangle + 0.27|-\tfrac{3}{2}\rangle + 0.85|+\tfrac{5}{2}\rangle,\\
|-\tfrac{1}{2}'\rangle &= -0.54|-\tfrac{1}{2}\rangle + 0.46|+\tfrac{3}{2}\rangle + 0.71|-\tfrac{5}{2}\rangle,\\
|+\tfrac{3}{2}'\rangle &= 0.44|+\tfrac{1}{2}\rangle - 0.76|-\tfrac{3}{2}\rangle + 0.48|+\tfrac{5}{2}\rangle,\\
|-\tfrac{3}{2}'\rangle &= 0.24|-\tfrac{1}{2}\rangle - 0.72|+\tfrac{3}{2}\rangle + 0.65|-\tfrac{5}{2}\rangle,\\
|+\tfrac{5}{2}'\rangle &= 0.77|+\tfrac{1}{2}\rangle + 0.60|-\tfrac{3}{2}\rangle + 0.22|+\tfrac{5}{2}\rangle,\\
|-\tfrac{5}{2}'\rangle &= 0.81|-\tfrac{1}{2}\rangle + 0.52|+\tfrac{3}{2}\rangle + 0.28|-\tfrac{5}{2}\rangle. \qquad (2)
\end{aligned}
$$

While the relations among the coefficients of each superposition state look somewhat ambiguous, it is clear that there exist two groups of superposition states, each of which consists of three identical basis vectors without a common one among them. Specifically, when the Hamiltonian is modified to have the strongest possible off-diagonal coupling (i.e., at 90°), the

total number of symmetries of eigenstates is essentially reduced to two, the minimum number of symmetries in the presence of the Zeeman interaction. Equation (2) also tells us that the states of each pair $|\pm m'\rangle$ have opposite symmetries and thus should not interact with each other near 90°. Given this, the significant increase (decrease) of the energy splitting between $|\pm\frac{1}{2}'\rangle$ ($|\pm\frac{3}{2}'\rangle$ or $|\pm\frac{5}{2}'\rangle$) with increasing θ towards 90°, as shown in Fig. 1(g), may seem puzzling. Note that the vanishing of the $\pm\frac{1}{2}' \leftrightarrow \pm\frac{3}{2}'$ transitions at 90° is explained well by the fact that the selection rule $\Delta m = \pm 1$, which holds as long as the set of basis states $|m\rangle$ is unaltered, cannot be satisfied between any superposition states with like symmetry.

It is important to realize that the fully cooperative mixing of all basis states at 90° is very different from the two-state-like behavior induced at the small angle of 4°. This implies that there are infinitely many superposition states which can be readily accessed and modified through NMR-NQR measurements. One just needs to adjust the internal control parameter θ which governs all Hamiltonian matrix elements, under small external magnetic fields. Since the manipulation of quantum superpositions through the control of off-diagonal coupling and the energy-splitting gap is fundamental to quantum technologies, our findings in the multistate quantum system could contribute to various applications in quantum computation and quantum information. Specifically, our research could be valuable in the study of qudits, which are higher-dimensional quantum systems [25–30].

IV. CONCLUSION

We have presented an NMR-NQR study on the drastic effects of off-diagonal coupling on eigenstates and eigenvalues of a ^{121}Sb nuclear spin system in an antimony single crystal. By precisely tuning the angle θ between the electric field gradient and an external magnetic field, we have revealed two important observations, i.e., (i) a direct probing of an avoided level crossing under weak off-diagonal coupling and (ii) a detailed full evolution of nuclear transitions and the associated superposition states as a function of the angle in a small external magnetic field. The experimental results were in excellent agreement with exact diagonalization calculations, proving the ability to manipulate superposition states in a multistate quantum system as a function of a well-defined control parameter. Therefore, our work not only deepens the understanding of fundamental principles underlying quantum physics but also may hold the potential for advancements in quantum computation and quantum information processing.

ACKNOWLEDGMENTS

We thank Gwang-Hee Kim for fruitful discussion. This work was supported by a National Research Foundation of Korea grant funded by the Korea Government (MSIT) (Grant No. NRF-2020R1A2C1003817). Work at the Ames Laboratory was supported by the U.S. Department of Energy, Office of Science, Basic Energy Sciences, Materials Sciences and Engineering Division. The Ames Laboratory is operated for the U.S. Department of Energy by Iowa State University under Contract No. DE-AC02-07CH11358.

[1] J. von Neumann and E. P. Wigner, Über das verhalten von eigenwerten bei adiabatischen prozessen, Phys. Z. **30**, 467 (1929).

[2] J. von Neumann and E. Wigner, in *Quantum Chemistry: Classic Scientific Papers*, edited by H. Hettema (World Scientific, Singapore, 2000), pp. 25–31.

[3] L. D. Landau and E. M. Lifshitz, *Quantum Mechanics: Non-Relativistic Theory* (Pergamon, Oxford, 1965).

[4] C. Cohen-Tannoudji, B. Diu, and F. Laloe, *Quantum Mechanics* (Wiley-VCH, Berlin, 2019), Vol. 1.

[5] L. Pauling, *The Nature of the Chemical Bond and the Structure of Molecules and Crystals* (Cornell University Press, Ithaca, 1960).

[6] J. R. Rubbmark, M. M. Kash, M. G. Littman, and D. Kleppner, Dynamical effects at avoided level crossings: A study of the Landau-Zener effect using Rydberg atoms, Phys. Rev. A **23**, 3107 (1981).

[7] N. P. Armitage, E. J. Mele, and A. Vishwanath, Weyl and Dirac semimetals in three-dimensional solids, Rev. Mod. Phys. **90**, 015001 (2018).

[8] Y. Nakamura, Y. A. Pashkin, and J. S. Tsai, Coherent control of macroscopic quantum states in a single-Cooper-pair box, Nature (London) **398**, 786 (1999).

[9] S. Bertaina, S. Gambarelli, T. Mitra, B. Tsukerblat, A. Müller, and B. Barbara, Quantum oscillations in a molecular magnet, Nature (London) **453**, 203 (2008).

[10] R. Rouse, S. Han, and J. E. Lukens, Observation of Resonant Tunneling between Macroscopically Distinct Quantum Levels, Phys. Rev. Lett. **75**, 1614 (1995).

[11] L. Thomas, F. Lionti, R. Ballou, D. Gatteschi, R. Sessoli, and B. Barbara, Macroscopic quantum tunnelling of magnetization in a single crystal of nanomagnets, Nature (London) **383**, 145 (1996).

[12] J. R. Friedman, V. Patel, W. Chen, S. K. Tolpygo, and J. E. Lukens, Quantum superposition of distinct macroscopic states, Nature (London) **406**, 43 (2000).

[13] C. H. van der Wal, A. C. J. ter Haar, F. K. Wilhelm, R. N. Schouten, C. J. P. M. Harmans, T. P. Orlando, S. Lloyd, and J. E. Mooij, Quantum superposition of macroscopic persistent-current states, Science **290**, 773 (2000).

[14] K. R. Brown, C. Ospelkaus, Y. Colombe, A. C. Wilson, D. Leibfried, and D. J. Wineland, Coupled quantized mechanical oscillators, Nature (London) **471**, 196 (2011).

[15] A. Abragam, *The Principles of Nuclear Magnetism* (Oxford University Press, Oxford, 1961).

[16] C. P. Slichter, *Principles of Magnetic Resonance* (Springer, Berlin, 1990).

[17] C. Dimitropoulos, M. Maglione, and F. Borsa, Nuclear magnetic and quadrupole resonance in metallic powders in the presence of strong quadrupole interaction: Rhenium metal, Phys. Rev. B **37**, 3159 (1988).

[18] A. D. Bain, Exact calculation, using angular momentum, of combined Zeeman and quadrupolar interactions in NMR, Mol. Phys. **101**, 3163 (2003).

[19] M. Khasawneh, J. S. Hartman, and A. D. Bain, Direct detection of chlorine-35 multiple-quantum NMR transitions in a single crystal of sodium chlorate, Mol. Phys. **102**, 975 (2004).

[20] K. Raman, Asymmetry parameter studies for systems containing the ^{35}Cl nucleus from Zeeman NQR data, J. Mol. Struct. **345**, 31 (1995).

[21] B. H. Suits, in *Handbook of Applied Solid State Spectroscopy*, edited by D. R. Vij (Springer, Berlin, 2006), pp. 65–96.

[22] C. S. Barrett, P. Cucka, and K. Haefner, The crystal structure of antimony at 4.2, 78 and 298 K, Acta Cryst. **16**, 451 (1963).

[23] R. R. Hewitt and B. F. Williams, Nuclear quadrupole interaction of Sb^{121} and Sb^{123} in antimony metal, Phys. Rev. **129**, 1188 (1963).

[24] G. C. Carter, L. H. Bennett, and D. J. Kahan, *Metallic Shift in NMR* (Pergamon, New York, 1977).

[25] J. Teles, E. R. DeAzevedo, J. C. C. Freitas, R. S. Sarthour, I. S. Oliveira, and T. J. Bonagamba, Quantum information processing by nuclear magnetic resonance on quadrupolar nuclei, Philos. Trans. R. Soc. A **370**, 4770 (2012).

[26] S. Dogra, A. Dorai, and K. Dorai, Implementation of the quantum Fourier transform on a hybrid qubit-qutrit NMR quantum emulator, Int. J. Quantum Inf. **13**, 1550059 (2015).

[27] Z. Gedik, I. A. Silva, B. Çakmak, G. Karpat, E. L. G. Vidoto, D. O. Soares-Pinto, E. R. deAzevedo, and F. F. Fanchini, Computational speed-up with a single qudit, Sci. Rep. **5**, 14671 (2015).

[28] Y. Wang, Z. Hu, B. C. Sanders, and S. Kais, Qudits and high-dimensional quantum computing, Front. Phys. **8**, 589504 (2020).

[29] S. Carretta, D. Zueco, A. Chiesa, Á. Gómez-León, and F. Luis, A perspective on scaling up quantum computation with molecular spins, Appl. Phys. Lett. **118**, 240501 (2021).

[30] M. Atzori, E. Garlatti, G. Allodi, S. Chicco, A. Chiesa, A. Albino, R. D. Renzi, E. Salvadori, M. Chiesa, S. Carretta, and L. Sorace, Radiofrequency to microwave coherent manipulation of an organometallic electronic spin qubit coupled to a nuclear qudit, Inorg. Chem. **60**, 11273 (2021).